Braz J Phys (2016) 46:198–205
DOI 10.1007/s13538-016-0401-z

SOCIEDADE BRASILEIRA DE FÍSICA

CONDENSED MATTER

Structural and Fluctuation Induced Excess Conductivity in R:1113 Superconductors

A. Sedky[1] · **M. I. Youssif**[2]

Received: 27 June 2015 Published online: 16 February 2016

Abstract We report here the fluctuation-induced excess conductivity in $RBaSrCu_3O_{7-\delta}$ (R = Y, Gd, Nd, and La) superconductor. It is found that Y and Gd samples are orthorhombic, while the Nd and La samples are quasi-tetragonal. The oxygen content is found to be close to 7 for all R:1113 samples. The logarithmic plots of $\Delta\sigma$ and reduced temperature ϵ reveal two different exponents corresponding to crossover temperature due to shifting the order parameter from (2D/1D) to (3D). The critical temperature, mean field temperature, crossover temperature, out of plane coherence length, and interlayer coupling are decreased as the ionic size increases. While the in plane and effective coherence lengths, and anisotropy are increased. We have also estimated several physical parameters such as upper critical magnetic fields in both *a*-*b*- and *c*-axis (B_{ab} and B_C), and critical current density J (0 K), and their values are found to be decrease as the ionic size increases. The results are discussed in terms of oxygen rearrangement, localization of carriers, coherence lengths, and anisotropy which are produced as the ionic size increases.

Keywords Ceramics · Chemical synthesis · X-ray diffraction · Electrical properties · Transport properties

✉ A. Sedky
sedky1960@yahoo.com

[1] Physics Department, Faculty of Science, Assiut University, Assiut, Egypt

[2] Physics Department, Faculty of Science at New Damietta, Damietta University, New Damietta 34517, Egypt

1 Introduction

Since the discovery of high-temperature superconductors (HTSC), extensive studies have been done to clarify their superconducting nature [1]. One way to probe their mechanism is the investigation of their properties in the normal state region. These properties include the thermal energy-induced fluctuations in both phase and modulus of the superconducting order parameter around its mean field region [2–5]. Due to short coherence length together with elevated values of critical temperature in high-temperature superconductors, the thermal fluctuations of superconducting order parameter have been early observed in the conductivity versus temperature curves as excess conductivity [6]. By decreasing the temperature from room temperature toward the critical temperature T_c, the fluctuating of Cooper pairs begin to be created spontaneously at a temperature $T \geq 2T_c^{mf}$ [7–10]. As the temperature approaches T_c, the number of Cooper pairs increases, while the normal electron density decreases. Therefore, the resistivity decreases and the thermal fluctuations induce an excess conductivity $\Delta\sigma$ [11–13].

The fluctuation-induced conductivity (FIC) analyses reveal that the contribution of excess conductivity is due to Gaussian and critical fluctuations in the mean field and critical regions, respectively [14]. Gaussian fluctuation is probably dominant in the temperature region above the mean field temperature T_c^{mf} when the fluctuation in the order parameter is small and the interactions between Cooper pairs can be neglected, while the critical fluctuation occurs in the critical field region below the T_c^{mf} when the fluctuations in the order parameter are large and the interactions between Cooper pairs is considered. The variation of Gaussian fluctuation-induced conductivity with the reduced temperature helps the researchers to find the dimensional exponents, coherence length, and crossover temperatures [15, 16]. The dimensional exponents in high T_c

materials are found to be zero-dimensional (0D), one-dimensional (1D), two-dimensional (2D), and three-dimensional (3D). It is seen that the dimensional crossover takes place between any two different dimensional regions, and it is mainly obtained above T_c [17, 18].

However, the critical temperature T_c for all R:123 superconducting systems is 90 K at oxygen-deficient δ close to zero [19–25]. This means that the R ions remain in the trivalent state, and the T_c values are independent of the chosen R, in which the charge neutrality would require that the level of hole carriers in them remains the same for a particular family independent of the R ions. Based on the above, a 3D dimensional behavior is obtained close to T_c for all R:123 systems [26–28]. Unlike R:123, the R:1113 compounds crystalline in a either orthorhombic or tetragonal structure with oxygen content close to 7. But, T_c is changed by the chosen R especially in the case of R:124, R:247, and R:1113 superconducting systems. For example, T_c of Y:124 is about 80 K, but it is around 70 K for Nd:124 [26–32].

However, Y:1113 has been reported to crystalline in the orthorhombic R:123 structure with a T_c of around 82 K, and the T_c are decreased to 45 K as the ionic size increases to lighter R ions such as La [29]. In the present work, we address the question of Sr substitution at Ba site by studying the structural and superconducting properties of R:1113 system. Besides, in other substituted R-123 systems, a fluctuation study is reported to look may be for the first time the effects of Sr on the well-known 3D dimensionality of R:123. It would be also interesting to investigate the impact of rare earth ionic size on fluctuation and excess conductivity of the same series. However, we selected R = Y, Gd, Nd, and La in the $RBaSrCu_3O_7$ superconducting series as some representatives to cover nearly the entire lanthanide series, in order to look for structural and T_c behaviors through analysis of X-ray and R-T measurements. Further, we have used the data of R-T curves for fluctuation and excess conductivity study. We could also estimate several physical parameters such as upper critical magnetic fields in both *a*-*b*- and *c*-axis (B_{ab} and B_C), and critical current density J (0 K). The appearance of 1D conductivity for R = Gd, Nd, and La samples could be interpreted as evidence for the existence of conducting charge stripes in this type of copper oxide superconductors.

2 Experimental Details

A series of $RBaSrCu_3O_{7-\delta}$ (R = Y, Gd, Nd and La) samples are synthesized by the well-known solid state reaction method. The ingredients R_2O_3, $BaCO_3$, $SrCo_3$, and CuO of 4 N Purity are thoroughly mixed in required proportions and calcined at 900 °C in air for a period of 16 h, and then the furnace is slowly cooled to room temperature. This exercise is repeated three times with intermediate grinding at each stage. The resulting powders are ground, palletized in to pellets, and sintered at 940 °C for a period of 24 h. Finally, the furnace is cooled to room temperature with an intervening annealing for 24 h at 600 °C. After that, the samples are characterized for phase purity and oxygen deficient by X-ray diffraction (XRD) and iodometric titration. The electrical resistivity of the samples is obtained using the standard four-probe technique in closed cycle refrigerator [cryomech compressor package with cryostat Model 810–1812212, USA] within the range of (10–300) K. Nanovoltameter Keithley 2182, current source Keithley 6220, and temperature controller 9700 (0.001-K resolution) are used during these measurements.

3 Theoretical Background

The excess conductivity $\Delta\sigma$ due to thermal fluctuation is defined as the deviation of the measured conductivity of σ_m (T) from the normal conductivity σ_n (T) as follows:

$$\Delta\sigma = \left(\frac{1}{\rho_m} - \frac{1}{\rho_n}\right) = \sigma_m - \sigma_n \tag{1}$$

where ρ_m and ρ_n are the measured and normal resistivity, respectively. ρ_n is obtained from the measured resistivity ρ_m at $T \geq 2T_c$ by applying the least square method to the Anderson and Zou relation, $\rho_n(T) = A + BT$ [32]. In order to estimate the paraconductivity, Aslamazov and Larkin (AL) deduced the following relation for the fluctuation-induced excess conductivity $\Delta\sigma$ as [33]

$$\Delta\sigma = A\varepsilon^{-\lambda} \tag{2}$$

Here, $A = \frac{e^2}{32\hbar\xi_c(0)}$ for 3D, $A = \frac{e^2}{16\hbar d}$ for 2D, $A = \frac{e^2\xi_c(0)}{32\hbar S}$ for 1D, e is the electronic charge, d is the interlayer spacing between two successive CuO_2 planes, $\hbar$ is the reduced planks constant, ξ_c (0) is the *c*-axis 3D coherence length at zero temperature, S is the wire cross-sectional area of the 1D system, and λ is an exponent related with the actual conduction dimensionality D as $D = 2 + 2\lambda$. Values of the exponent's λ are 0.5, 1, and 1.5 for 3D, 2D, and 1D fluctuation, respectively, and ε is the reduced temperature given by [32–34]

$$\varepsilon = \frac{T - T_c^{mf}}{T_c^{mf}} \tag{3}$$

where T_c^{mf} is the mean field temperature; above it, the interactions between Cooper pairs can be neglected, the onset of superconducting phase coherence occurred.

We have followed the dρ/dT versus T plot to obtain the values of T_c^{mf} from the peaks.

However, for polycrystalline samples, the modified equations for 2D and 3D fluctuations are expressed as [35]

$$\Delta\sigma_{3D} = \frac{e^2}{32\hbar\xi_p(0)}\varepsilon^{-\frac{1}{2}} \tag{4a}$$

$$\Delta\sigma_{2D} = \frac{1}{4}\left\{\frac{e^2}{16\hbar d}\varepsilon^{-1}\left[1+\left(1+\frac{8\xi_c^4(0)}{d^2\xi_{ab}^2(0)}\varepsilon^{-1}\right)^{\frac{1}{2}}\right]\right\} \tag{4b}$$

where $\xi_{ab}(0)$ is the coherence length at 0 K across the ab-plane and $\xi_p(0)$ is the effective characteristic coherence length at 0 K.

On the other hand, the cross over behavior from 2D to 3D occurs at a temperature T_0 given by [34]

$$T_0 = T_c^{mf}\exp\left(\frac{2\xi_c(0)}{d}\right)^2 \tag{5}$$

where $\xi_c(0)$ is given by [36, 37]

$$\xi_c(0) = \left(\frac{dk^{\frac{1}{2}}}{2}\right) \tag{6}$$

where d is the c-axis for these type of samples [27] and k is the interlayer coupling expressed by [38]

$$k = \ln\left(\frac{T_0}{2T_c^{mf}}\right) \tag{7}$$

4 Results and Discussion

Figure 1 shows the XRD pattern of R:1113 samples. It is clear that Y and Gd samples are orthorhombic being evident from crystallographic splitting of (006), (200) and (116), and (213), while Nd and La samples are quasi-tetragonal. There are few impurity lines in the XRD patterns arising from the small amounts of R:211 and R_2O_3 phases. The values of orthorhombic distortion (OD) against ionic size are listed in Table 1 (the ionic size of the samples are 1.02 , 1.06, 1.12, and 1.18 Å for Y, Gd, Nd, and La samples, respectively). It is clear that OD is generally decreased as ionic size increases. The oxygen content listed in Table 1 is found to be close to 7 for all R:1113 samples.

Because the OD are significantly decreased for Nd and La samples, the neutron diffraction analysis based on these samples shows a rearrangement of O(1) and O(5) site occupancies in the Cu-O chains in such a way that both are nearly equally occupied without intermixing between Sr and Ba [38]. This is obtained only for bigger ionic size of rare earths (higher c-axis), which is consistent with OD behavior listed in Table 1. A similar behavior has been observed for La:1113 superconductors when Sr is replaced by Ca [39].

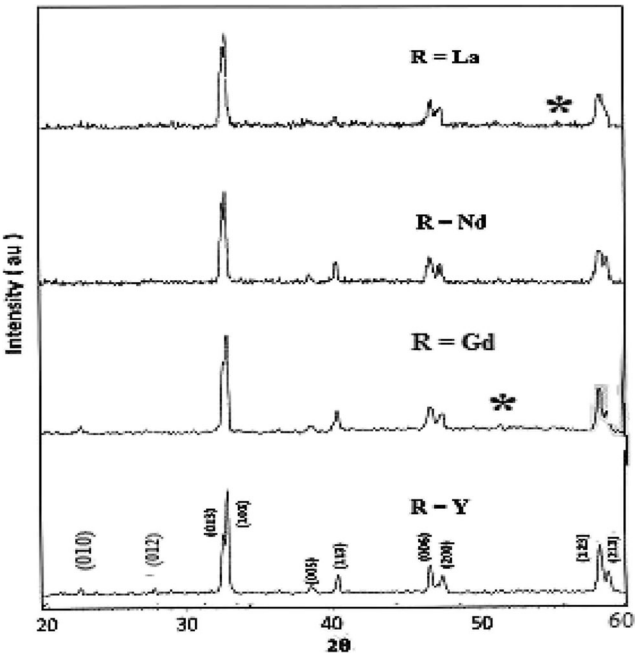

Fig. 1 X-ray diffraction pattern for $RBaSrCu_3O_{7-\delta}$ samples

The curves of resistivity versus temperature for the samples are given in Fig. 2a–d. The normal resistivity is linear as the temperature reduced from room temperature down to a certain temperature T_B. In this region, $\rho_n(T)$ follows the above formula, $\rho_n(T) = A + BT$ as discussed above. $T_B \simeq 2T_c^{mf}$ is defined as the temperature below which the Cooper-pair formation starts [40–42]. As the temperature is further reduced beyond the normal state region, the rate of change of resistivity becomes entirely different as compared to this region. This is mainly due to increasing Cooper pair formation as the temperature is reduced. Therefore, the fluctuation induced conductivity in this region follows the A-L model to yield the dimensional exponent appropriate to fluctuation-induced conductivity. As seen from the resistivity curves, the resistivity increases with increasing the ionic size, which suggest a weakening of the metallic behavior as the ionic size increases.

Table 1 OD, c-parameter, oxygen deficient δ, T_c, T_c^{mf}, T_0, λ_{3D}, D (3D), λ_{2D} and D (2D/1D) for $RBaSrCu_3O_{7-\delta}$ samples with various R

R	OD	c (Å)	δ	T_c (K)	T_c^{mf} (K)	T_o (K)	λ (3D)	D (3D)	λ 2D/1D	D (2D/1D)
Y	0.015	11.522	0.04	84	86.8	109	0.44	2.88	0.75	3.50
Gd	0.009	11.538	0.03	72	78.6	104	0.56	3.12	1.36	4.72
Nd	0.005	11.547	0.05	73	75.2	101	0.69	3.38	2.27	6.54
La	0.002	11.564	0.02	48	53.5	74.8	0.76	3.52	2.75	7.50

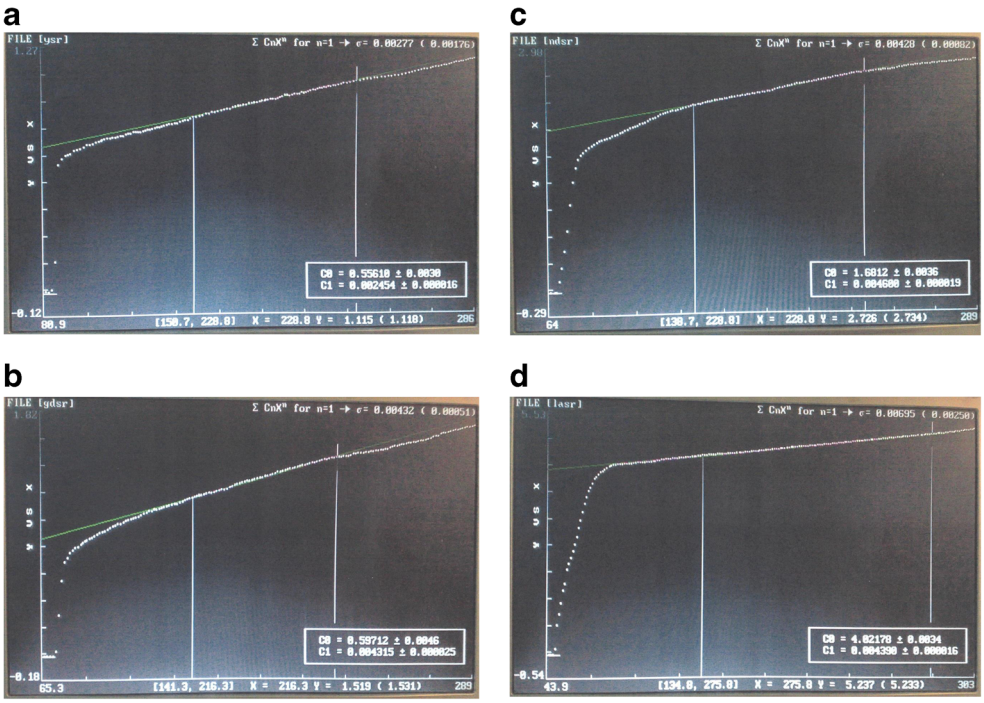

Fig. 2 **a**–**d** Resistivity versus temperature for $RBaSrCu_3O_{7-\delta}$ samples (**a** R = Y, **b** R = Gd, **c** R = Nd and **d** R = La)

The normal resistivity $\rho_n(T)$ is calculated in terms of A and B parameters which are obtained from the linear fit of the measured resistivity. The mean field temperatures T_c^{mf} for all samples are estimated from the peak of dρ/dT against temperature plot shown in Fig. 3. After that, we have calculated the excess conductivity $\Delta\sigma$ and reduced temperature ε. Then, we have plotted ln $\Delta\sigma$ against ln ε for all samples as shown in Fig. 4. It is evident from the fitting that there is distinct change in the slope of each plot. The corresponding temperature where the slope change occurs is designated as the crossover temperature T_o.

Figure 5a shows the variation of T_c, T_o, and T_c^{mf} against ionic size, and similar values are listed in Table 1. It is clear that T_c, T_c^{mf}, and T_o are decreased by increasing ionic size. However, two different exponents corresponding to crossover temperature are obtained from each plot with an accuracy of ±1 K. The first exponent occurred in the normal field region at and its values are between 1 and 2, in which the OPD is 2D/1D, while the second exponent occurred in the mean field region and its values are close to 0.5, in which the OPD is 3D ($-7.68 \le \ln \varepsilon \le -2.6$) and ($-2.6 \le \ln \varepsilon \le -0.88$) for Y, ($-3.96 \le \ln \varepsilon \le -1.22$) and ($-1.17 \le \ln \varepsilon \le -0.10$) for Gd, ($-3.90 \le \ln \varepsilon \le -1.07$) and ($-0.94 \le \ln \varepsilon \le -0.31$) for Nd, and ($-8.22 \le \ln \varepsilon \le -2.77$) and ($-2.11 \le \ln \varepsilon \le -0.71$) for La. Figure 5b shows the variation of OPD against ionic size, and similar values are listed in Table 1. The OPD is shifted from (2D) to (3D) as the temperature is reduced toward T_c. However, more than one region has been reported in pure and doped Y:123 samples [27, 43]. Normally, the critical field region is controlled by the critical fluctuation results from the small mean free path of the charge carriers and also the short coherence length produced as the carrier concentration is changed [27, 44–46]. Anyhow, the dimensional nature in RE:123 systems is supposed to be 3D conduction, but in some recent studies based on Y:123 superconductors, the presence of 2D fluctuation conduction is certified. Furthermore, an intermediate crossover region between 2D and 3D is reported for Y:123 systems, in agreement with the present work [47–49].

For polycrystalline samples, $\xi_p(0)$ is given by [36]

$$\frac{1}{\xi_p(0)} = \frac{1}{4}\left[\frac{1}{\xi_c(0)} + \left(\frac{1}{\xi_c^2(0)} + \frac{8}{\xi_{ab}^2(0)}\right)^{\frac{1}{2}}\right] \tag{8}$$

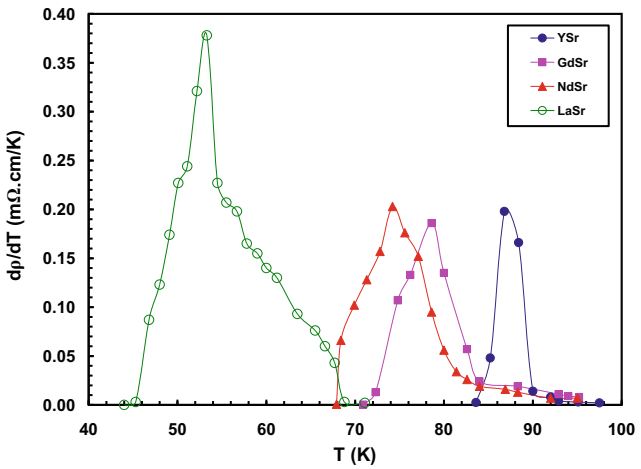

Fig. 3 dρ/dT versus temperature for $RBaSrCu_3O_{7-\delta}$ samples

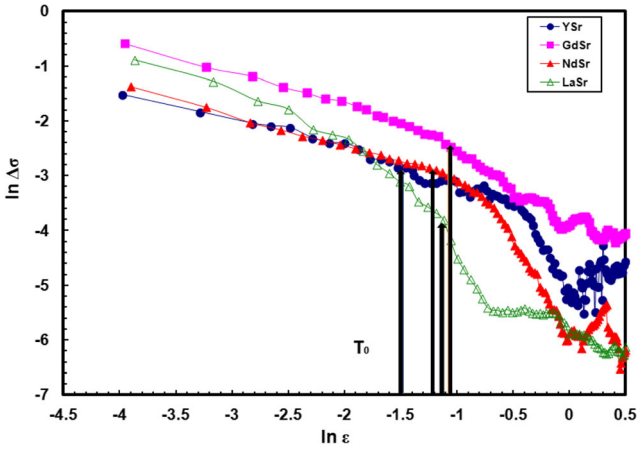

Fig. 4 Ln $\Delta\sigma$ against Ln ε for $RBaSrCu_3O_{7-\delta}$ samples

where ξ_{ab} (0) is calculated in terms of $\xi_p(0)$ and $\xi_c(0)$ values. Then, anisotropy parameter $\gamma = \frac{\xi_{ab}(0)}{\xi_c(0)}$ is easily obtained. Figure 5c shows the behaviors of $\xi_c(0)$, $\xi_{ab}(0)$, and $\xi_p(0)$ parameters against ionic radius. It is clear that the coherence lengths are generally increased as the ionic size increases. However, the variation of k and γ against ionic size is shown in Fig. 5b, and similar values are listed in Table 2. Actually, the R:1113 system is essentially 3D with two Cu-O_2 planes and one CuO chain which are manifested in the higher values of k and lower degree of anisotropy γ [50]. However, the decrease of k against ionic size suggested that the system may become higher anisotropy and consequently the charge carriers increasingly confined within the CuO_2 planes. The upper critical fields along the c-axis and a-b plane, and critical current density at 0 K J (0 K) are estimated by the following relations [51, 52]:

$$B_{II}(c) = \frac{\phi_0}{2\pi\xi_{ab}^2(0)} \quad , \quad B_{II}(ab) = \frac{\phi_0}{2\pi\xi_c(0)\xi_{ab}(0)} \tag{9}$$

$$J_c(0) = \frac{2\phi_0}{\sqrt{6}\pi\lambda^2(0)\ \xi_p(0)} \tag{10}$$

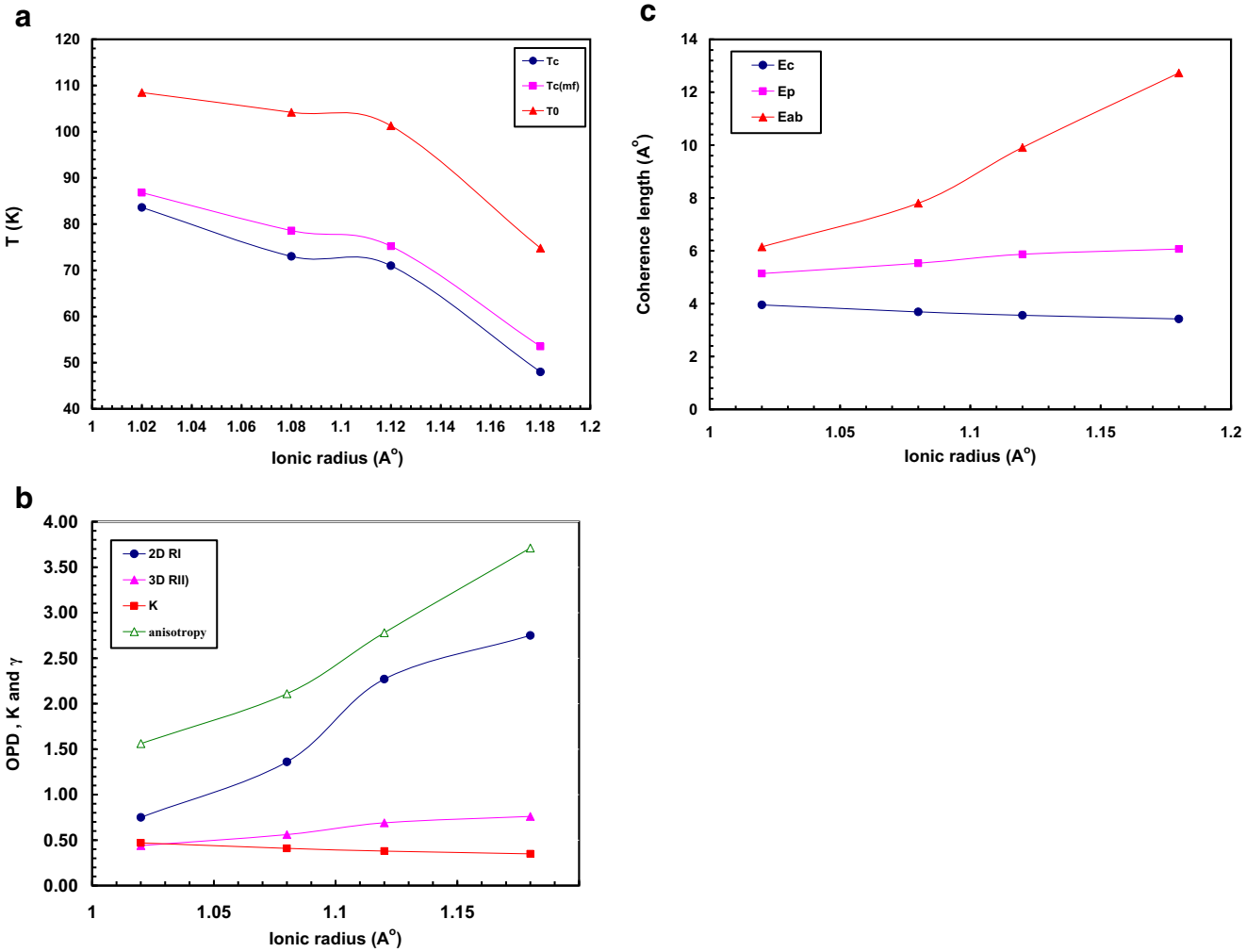

Fig. 5 **a** T_c, T_c^{mf}, and T_o versus ionic radius for $RBaSrCu_3O_{7-\delta}$ samples. **b** Order parameter, interlayer coupling, and anisotropy versus ionic radius for $RBaSrCu_3O_{7-\delta}$ samples. **c** Coherence lengths versus ionic radius for RBaSrCu3O7-δ samples

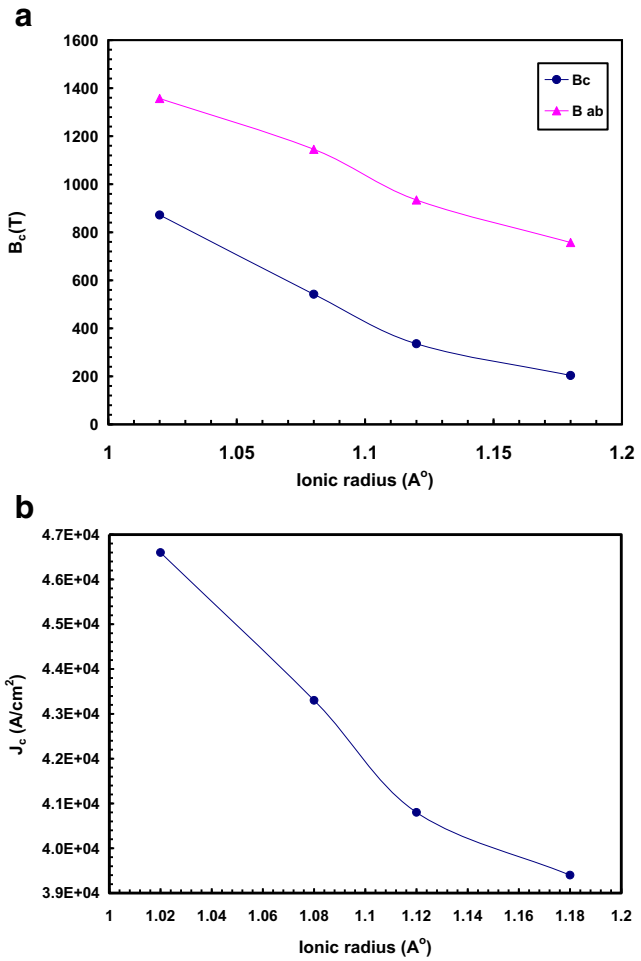

Fig. 6 **a** Critical magnetic fields versus ionic radius for $RBaSrCu_3O_{7-\delta}$ samples. **b** Critical current density versus ionic radius for $RBaSrCu_3O_{7-\delta}$ samples

where ϕ_0 is the quantum flux given by $\phi_0 = \frac{h}{2e} = 2.07 \times 10^{-15}(web/m^2)$ and $\lambda^2(0)$ is the London penetration depth at 0 K which is about 150 nm for R:123 superconductors [53]. The behaviors of B against ionic size are shown in Fig. 6a, and similar values are listed in Table 2. It is clear that B_{ab} is more than twice B_c, and their values are decreased as the ionic size increases, while critical current density J (0 K) shown in Fig. 6b is generally decreased by increasing ionic size.

However, we do not expect any changes in the London depth at 0 K according to the formula, $\lambda(T) = \lambda(0)\left[1-\frac{T}{T_c}\right]^{-\frac{1}{2}}$. At $T=T_c$, $\lambda(T)=0$, and at $T=0$, $\lambda(T)=\lambda(0)$ for all samples. But, the coherence lengths at 0 K $\xi^2_{ab}(0)$, $\xi_p(0)$, and $[\xi_c(0)\xi_p(0)]$ listed in Table 2 are increased as the ionic size increases and help for improving anisotropy of the lighter ions. This is of course a good real evidence in our hands for decreasing the critical fields and current for the lighter ions. The alternative way may be due decreasing zero temperature pinning potentials $\beta I(0)$ for the lighter ions which is 76.7×10^{-4} J/W for Er:123 systems. This is of course due to oxygen rearrangements and OD which helps for lowering the J_c (0 K) [54].

However, It is found that Cu atom in the CuO chains lose some of oxygen atoms as the ionic size increases, and consequently, the Cu coordination number is decreased. So, a slight change of superconducting transition temperature T_c is observed for the lower values of ionic size (R = Y, Gd). But, the further increase of ionic size leads to the abrupt decreasing of T_c, and the structure from orthorhombic to tetragonal phase occurs, in agreement with the present data for R = Nd and La [55–57].

Anyhow, a much increase in the OPD near the critical field region is observed for Nd and La samples, which suggested an anomalous crossover as a result of suppression of superconductivity as compared to Y sample. An indication of 2D near T_c suggests a deterioration in the CuO_2 coupling in this region. Furthermore, the increase of ionic size causes an increase in the c-axis coherence length, resulting in an increase of the mean free path, and consequently, the coupling between CuO_2 planes is decreased, while Y and Gd samples look more 3D near the critical field region and 2D/1D above the mean field region. Therefore, we do not expect decoupling of the CuO chains or an increase in ξ_c or c-axis length, which causes an increase in $\Delta\sigma$ [58]. Hence, the behavior of these samples is nearly similar to the pure Y:123 sample, and the planes remain coupled as strongly.

Because of the matching ionic radii and divalent oxidation states, substitutions of Sr for Ba in R:113 systems are not likely to have any significant effect on the carrier density. The Ba and Sr ions have the same valence states, and the charge balance within the CuO_2 plane does not change. On the other hand, the increase of ionic size from Y up to La may be disorders and disturbs the hybridization and alignment between Cu-3d and O-2p, and causes the carrier localization in the CuO_2 planar networks. Furthermore, in London criteria, $n_s(0) \propto \lambda^{-2}(0)$, the $\lambda(0)$ increase corresponding to a large

Table 2 k, ξ_c (0), ξ_{ab} (0), ξ_c (0)ξ_{ab} (0), γ, ξ_p (0), B_{IIC}, B_{IIab} and J(0) for $RBaSrCu_3O_{7-\delta}$ samples with various R

R	k	ξ_c (0) (Å)	ξ_{ab}(0) (Å)	ξ_c (0)ξ_{ab}(0) (Å)^2	γ	ξ_p (0) (Å)	B_{IIC} (T)	B_{IIab} (T)	J (A/cm^2)
Y	0.47	3.95	6.15	24.29	1.56	5.14	871.5	1357	4.66×10^4
Gd	0.41	3.69	7.80	28.78	2.11	5.53	541.8	1145	4.33×10^4
Nd	0.38	3.56	9.91	35.28	2.78	5.87	335.6	934.3	4.08×10^4
La	0.35	3.42	12.7	43.43	3.71	6.07	203.4	757.1	3.94×10^4

decrease in carrier density n_s is reported [59, 60]. Therefore, the invariant of OPD with ionic size suggests its independence from n_s variation, while the OD independent of Sr indicates an intact oxygen ordering or the linear chain structure. Since Sr does not change the lattice parameters significantly, we neither expect a change in the overlap between the Cu-3d and O-2p orbital's nor in the separation between the CuO_2 planes. The 3D nature of the OPD and its invariance by Sr indicate that the two planes in the unit cell are so coupled that their contributions appear as due to a single plane, vice versa in the case of R ions. However, appearance of the 1D fluctuation in the superconductivity process in these types of high T_c materials suggests that the CuO chains are also contributed in the electrical conducting as well as the CuO_2 planes [51, 52].

The mean-field region for each sample consists of three distinct linear parts indicating 1D, 2D, and 3D fluctuation conductivity behavior. It is well-known that inhomogeneities and characteristics of superconducting grain crucially influence the mean-field regimes and the dimensionality of fluctuation conductivity [61, 62]. 1D fluctuation conductivity appearing in our samples suggests the existence of 1D-conducting channels. Similar behaviors are also observed in HTS materials [63–66]. The 1D regime fluctuation has been interpreted by the existence of conducting charge stripes in the superconducting cuprate [67]. This model incorporates electronic and magnetic structural features; the system is inhomogeneous and charge segregation into domain walls that are separated by antiferromagnetic insulating zones. Notably, the width of the 1D region is increasing sharply for Nd and La samples compared to Y and Gd. This may suggest that oxygen rearrangements and the higher anisotropy presented in the Nd and La samples destabilize the conducting charge stripes. Therefore, the width of the 2D/1D regime is wider for the Nd and La samples, in which 1D is clearly obtained.

5 Conclusion

Structural and fluctuation-induced excess conductivity in $RBaSrCu_3O_{7-\delta}$ (R1113) superconductors is reported. Y and Gd samples are orthorhombic, while the Nd and La samples are quasi-tetragonal. The oxygen content is found to be close to 7 for all R:1113 samples. The fluctuation conductivity analysis revealed the occurrence of two fluctuation regions corresponding to 2D/1D and 3D for all samples. We have shown a decrease in the critical temperature, mean field temperature, crossover temperature, out of plane coherence length, and interlayer coupling as the ionic size increases, while the in plane and effective coherence lengths, and anisotropy are increased. The appearance of 1D conductivity for R = Gd, Nd, and La samples could be interpreted as evidence for the existence of conducting charge stripes in this cuprate. Moreover, the upper critical magnetic fields and critical current density J (0 K) are decreased as the ionic size increases. A rearrangement of O(1) and O(5) and an increase of both coherence lengths anisotropy are investigated as the ionic size increases.

Acknowledgments The R-T measurements are done by authors during their work at KFU and KSU Universities, Saudi Arabia (2002–2013). While the XRD, fluctuation analysis, article preparations and article submission and revisions are done by the authors in Egypt (2013-2015). The authors would like to thank the KFU and KSU Universities for providing facilities and maintenance support during the measurements.

References

1. J.S. Shier, D.M. Ginsberg, Phys. Rev. B **147**, 384 (1966)
2. P.P. Freitas, C.C. Tsuei, T.S. Plaskett, Phys. Rev. B **36**, 833 (1987)
3. M. Daemling, J.M. Seuntjens, D.C. Larbalestier, Nature **346**, 332 (1990)
4. J. Rosenblatt, P. Peyral, A. Raboutou, C. Lebeau, Physica B **152**, 95 (1988)
5. P. Pureur, J. Schaf, M.A. Gusmão, J.V. Kunzler, Physica C **176**, 357 (1991)
6. M.R. Cimberle, C. Ferdeghini, E. Giannini, D. Marre, M. Putti, A. Siri, F. Federici, A. Varlomov, Phys. Rev. B **55**, 14745 (1997)
7. A. Harabor, N.A. Harabor, M. Deletter, J. Optoelectron. Adv. Mater. **8**, 1072 (2006)
8. A. Mohanta, D. Behera, Physica C **470**, 295 (2010)
9. D.S. Fisher, M.P.A. Fisher, D.A. Huse, Phys. Rev. B **43**, 130 (1991)
10. D.K. Aswal, A. Singh, S. Sen, M. Kaur, C.S. Viswandham, G.L. Goswami, S.K. Gupta, J. Phys. Chem. Solids **63**, 1797 (2002)
11. M. Sahoo, D. Behera, J. Phys. Chem. Solids **74**, 950 (2013)
12. A. Esmaeili, H. Sedghi, J. Alloys Compd. **537**, 29 (2012)
13. E.M.M. Ibrahim, S.A. Saleh, Supercond. Sci. Technol. **20**, 672 (2007)
14. K. Maki, R.S. Thompson, Phys. Rev. B **39**, 2767 (1988)
15. F. Vidal, J.A. Veira, J. Maja, J.J. Ponte, F.G. Alvarado, E. Mordan, J. Amador, C. Cascales, Physica C **156**, 807 (1988)
16. F. Ben Azzouz, M. Annabi, M. Zouaoui, M. Ben Salem, Phys. Status Solidi C **9**, 2978 (2006)
17. C. Baraduc, V. Pagnon, A. Buzdin, J. Henry, C. Ayache, Phys. Lett. A **166**, 267 (1992)
18. U.K. Mohapatra, R. Biswal, D. Behera, N. Mishra, Supercond. Sci. Technol. **19**, 635 (2006)
19. P.H. Hor, R.L. Meng, J. Bechtold, K. Forster, C.W. Chu, Phys. Rev. Lett. **58**, 1891 (1987)
20. M. Guillaume, M. Shirai, N. Suzuki, K. Motizuki, J. Phys. Condens. Matter **6**, 7963 (1994)
21. G.V.M. Williams, J.L. Tallon, Physica C **258**, 41 (1994)
22. H. Lütgemeier, S. Schmenn, P. Meuffels, O. Storz, R. Schöllhorn, C. Niedermayer, I. Heinmaa, H. Yu, Physica C **267**, 191 (1996)
23. H.A. Blackstead, J.D. Dow, D.B. Chisey, J.S. Horwitz, M.A. Black, P.J. McGinn, A.E. Klunzinger, D.B. Pulling, Phys. Rev. B **54**, 6122 (1996)
24. H. Oesterreicher, M. Smith, Mater. Res. Bull. **22**, 1709 (1987)
25. L. Soderholm, K. Zhang, D.G. Hinks, M.A. Beno, J.D. Jorgensen, C.U. Segre, I.K. Schuller, Nature **328**, 604 (1987)
26. U. Welp, in *High Temperature Superconductivity*, ed. by S.K. Malik, S.S. Shah (Nova Science, New York, 1992)
27. A. Sedky, J. Low Temp. Phys. **148**, 53 (2007)
28. W. Loram, J.M. Wheatley, K.A. Mirza, R.S. Liu, Philos. Mag. B **65**, 1405 (1992)

29. V.P.S. Awana, S.K. Malik, A. Claudio, O.F. Delima, G. Anurag, A. Sedky, W.B. Yelon, P. Ram, A.V. Narlikar, Mod. Phys. Lett. B **14**(10), 361 (2000)
30. V.P.S. Awana, V.P.S. Awana, O.F. de Lima, S.K. Malik, W.B. Yelon, A.V. Narlikar, Physica C **314**, 93 (1999)
31. S.K. Agarwal, R. Lal, V.P.S. Awana, S.P. Pandey, A.V. Narlikar, Phys. Rev. B **50**, 10265 (1994)
32. R.G. Buckley, J.L. Tallon, D.M. Pooke, M.R. Presland, Physica C **165**(391) (1990)
33. A. Das, R. Suryanarayanan, J. Physique **15**, 623 (1995)
34. W. Anderson, Z. Zou, Phys. Rev. Lett. **60**, 132 (1988)
35. L.G. Aslamazov, A.I. Larkin, Phys. Lett. A **26**, 238(1968); Sov.Phys. Solid State **10**, 875 (1968)
36. W.E. Lawrence, S. Doniach, S. Proc. 12^{Th} Int. Conf. Low Temp. Phys. Kyoto, 1970 (Edited by E. Kanada), (Keigaku, Tokyo, 1971), p. 361
37. A.K. Gosh, S.K. Bandyopadhyay, A.N. Basu, J. Appl. Phys. **86**, 3247 (1999)
38. A.K. Ghosh, S.K. Bandyopadhyay, P. Barat, S. Pintu, A.N. Basu, Physica C **264**, 255 (1996)
39. M.V. Ramallo, C. Torron, F. Vidal, Physica C **230**, 97 (1994)
40. C. Baraduc, A. Bazdin, Phys. Lett. A **171**, 408 (1992)
41. A.K. Ghosh, S.K. Bandyopadhyay, P. Barat, S. Pintu, A.N. Basu, Physica C **319**, 255 (1995)
42. L. Reggiani, R. Vaglio, A.A. Varlamov, Phys. Rev. B **44**, 9541 (1991)
43. F. Vidal, J.A. Veira, J. Maza, F. Garcia- Alvarado, E. Moran, M.A. Alario, J. Phys. C **21**, L9 (1988)
44. J.A. Veira, J. Maza, F.J. Vida, Phys. Lett. A **131**, 310 (1988)
45. A.K. Ghosh, S.K. Bandyopadhyay, A.N. Basu, Mod. Phys. Lett. B **11**, 1013 (1997)
46. A.K. Ghosh, A.N. Basu, Supercond. Sci. Technol. **13**, 343 (2000)
47. S.N. Bhatia, C.P. Dhard, Phys. Rev. B **49**, 12206 (1994)
48. M.P. Rojas Sarmiento, M.A. Uribe Laverde, E. Vera Lopez, D.A. Landinez Tellez, J. Roa-Rojas, Physica B **398**, 360 (2007)
49. R.V. Vovk, M.A. Obolenskii, A.V. Bondarenko, I.L. Goulatis, A. Chroneos, Acta Phys. Pol. **111**, 129 (2007)
50. P. Mandal, A. Poddar, A.N. Das, J. Phys Condens. Matter **6**, 5689 (1994)
51. S.R. Ghorbani, M. Homaei, Mod. Phys. Lett. B **25**(23), 1915 (2011)
52. K. Nawazish Ali, H. Najmul, N. Sana, S. Babar, K. Sajid, A.A. Rizvi, J. Appl. Phys. **107**, 083910 (2010)
53. Y. Petrovie, R. Fasano, M. Lortz, M. Dcrous, M. Potel, R. Cheriel, Physica C. **460**–**462**,702 (2007)
54. B.V. Kumaraswamy, R. Lal, A.V. Narlikar, Phys. Rev. B **52**, 1320 (1995)
55. R. Wordenweber , K. Heinemann , G.V.S. Sastry, H.C. Freyhardt, Physica C. **162**–**164**, 1601(1989)
56. R.A. Asaturian, A.G. Sarkissian, E.L. Ignatian, K.G. Begoian, Solid State Commun. **95**, 389 (1995)
57. J.R. Cooper, S.D. Obretelli, P.A. Freeman, Zheng, Supercond. Sci. Technol. **4**, S277 (1991)
58. S. Rusiecki, B. Bucher, E. Kaldis, E. Jilek, J. Karpinski, J. Less-Common Met. **31**, 164–165 (1990)
59. E.R. Ulm, J.T. Kim, T.R. Lemberger, S.R. Foltyn, X. Wu, Phys. Rev. B **51**, 9193 (1995)
60. A. Porch, J.R. Cooper, D.N. Zheng, J.R. Waldram, Physica C **214**, 350 (1993)
61. E. Hannachi, Y. Slimani, M.K. Ben Salem, A. Hamrita, D.K. Mani, M. Ben Salem, F. Ben Azzouz, Mater. Chem. Phys. **159**, 185 (2015)
62. A.I. Abou Aly, N.H. Mohammed, R. Awad, H.A. Motaweh, D. El-Said Bakeer, J. Supercond. Nov. Magn. **25**, 2281 (2012)
63. I. Bouchoucha, F. Ben Azzouz, M. Ben Salem, J. Supercond. Nov. Magn. **24**, 345 (2011)
64. A.I. Abou-Aly, R. Awad, I.H. Ibrahim, W. Abdeen, Solid State Commun. **149**, 281 (2009)
65. T. Sato, H. Nakane, S. Yamazaki, N. Mori, S. Hirano, S. Yoshizawa, T. Yamaguchi, Physica C **643**, 392 (2003)
66. T. Sato, H. Nakane, S. Yamazaki, N. Mori, Physica C **1208**, 372 (2002)
67. A. Bianconi, A. Valletta, A. Perali, N.L. Saini, Physica C **296**, 269 (1998)